8. D. J. Schaefer *et al.*, *Macromolecules* **28**, 1152 (1995).
9. M. T. Hansen, C. Boeffel, H. W. Spiess, *Colloid Polym. Sci.* **271**, 446 (1993).
10. L. S. Loo, R. E. Cohen, K. K. Gleason, *Macromolecules* **32**, 4359 (1999).
11. N. S. Murthy, M. Stamm, J. P. Sibilia, S. Krimm, *Macromolecules* **22**, 1261 (1989).
12. J. Hirschinger, H. Miura, A. D. English, *Macromolecules* **23**, 2153 (1990).
13. J. L. Hutchison, N. S. Murthy, E. T. Samulski, *Macromolecules* **29**, 5551 (1996).
14. E. O. Stejskal and J. Schaefer, *J. Magn. Reson.* **14**, 160 (1974).
15. D. I. Hoult and R. E. Richards, *Proc. R. Soc. London Ser. A* **344**, 311 (1975).
16. R. E. Robertson, *J. Chem. Phys.* **44**, 3950 (1966).
17. D. Deng, A. S. Argon, S. Yip, *Philos. Trans. R. Soc. London. Ser. A* **329**, 613 (1989).

18. We thank A. S. Argon for helpful discussions. This work made use of the Materials Research Science and Engineering Centers (MRSEC) Shared Facilities supported by NSF under award DMR-9400334. This work was supported primarily by the MRSEC Program of NSF under award DMR 98-08941.

24 November 1999; accepted 9 February 2000

Low (Sub–1-Volt) Halfwave Voltage Polymeric Electro-optic Modulators Achieved by Controlling Chromophore Shape

Yongqiang Shi,[1] Cheng Zhang,[2] Hua Zhang,[3] James H. Bechtel,[1] Larry R. Dalton,[2,4] Bruce H. Robinson,[4] William H. Steier[3]

Electro-optic (EO) modulators encode electrical signals onto fiber optic transmissions. High drive voltages limit gain and noise levels. Typical polymeric and lithium niobate modulators operate with halfwave voltages of 5 volts. Sterically modified organic chromophores have been used to reduce the attenuation of electric field poling–induced electro-optic activity caused by strong intermolecular electrostatic interactions. Such modified chromophores, incorporated into polymer hosts, were used to fabricate EO modulators with halfwave voltages of 0.8 volts (at a telecommunications wavelength of 1318 nanometers) and to achieve a halfwave voltage-interaction length product of 2.2 volt-centimeters. Optical push-pull poling and driving were also used to reduce halfwave voltage. This study, together with recent demonstrations of exceptional bandwidths (more than 110 gigahertz) and ease of integration (with very large scale integration semiconductor circuitry and ultra-low-loss passive optical circuitry) demonstrates the potential of polymeric materials for next generation telecommunications, information processing, and radio frequency distribution.

Electro-optic (EO) polymers have been under development for several years (*1*). The interest in these materials derives from the need for high-speed (wide bandwidth), low-drive-voltage, EO modulators for fiber optic communication links, in which the modulator encodes an electrical driving signal onto an optical transmission beam. Improvement in link performance depends on decreasing the halfwave voltage (V_π), because link gain is inversely proportional to V_π^2 and the noise figure is directly proportional to V_π^2 in the low-gain limit (*2*). In earlier work, Teng (*3*) demonstrated a traveling wave polymer modulator at 40 GHz. Recently, polymer modulators have been demonstrated operating at over 100 GHz and $LiNbO_3$ modulators at over 70 GHz (*3*, *4*). However, in each case the required radio frequency (rf) drive voltage has remained persistently high ($V_\pi \sim 5$ V) (*3*, *4*). The "holy grail" of the wide bandwidth optical modulator field is a $V_\pi < 1$ volt device, which would make the distribution of millimeter wave signals via photonic techniques practical and would significantly increase the efficiency of fiber optic (and satellite) communication systems. Although the focus of this report is on improvement of V_π voltages realized for polymeric modulators, we note that implementation of clever modulator designs has permitted the extension of interaction lengths for lithium niobate modulators with a corresponding reduction in V_π (*5*). In the case of polymeric materials, current improvements reflect (and future improvements will likely continue to reflect) the development of improved materials as well as improved device concepts.

Chromophore-containing polymeric materials have held the promise of exceptionally high EO coefficients (r_{33}) through the systematic chemical design of chromophores with large hyperpolarizability (β), but unanticipated problems in translating microscopic to macroscopic optical nonlinearity have slowed progress. Great progress has been made in understanding the molecular origins of hyperpolarizability, and many molecules exhibiting exceptional β values have been synthesized (*1*, *6*). It has, however, been difficult to incorporate these molecules into a host material with sufficient noncentrosymmetric molecular alignment to achieve device-appropriate EO activity. Recent theoretical analysis by Dalton *et al.* (*1*, *7*) has shown that the dipole-dipole interactions among chromophores makes it impossible to achieve a high degree of noncentrosymmetric order unless undesirable spatially anisotropic intermolecular electrostatic interactions are minimized by modification of the shape of chromophores to sterically inhibit such interactions. Here we report the realization of a $V_\pi \sim 0.8$ V and a $V_\pi L$ (voltage interaction length) product ~ 2.2 V·cm in optical intensity modulators using a new, structurally modified, highly nonlinear optical chromophore, CLD-1 (*8*) (Figs. 1 and 2). Recently, comparable results have been achieved by researchers at Lockheed-Martin Corporation (*9*) using an FTC-type chromophore (Figs. 1 and 2).

Traditional EO polymer modulators use a Mach-Zehnder interferometer architecture with only one arm modulated with a microstripline electrode (*3*, *10*, *11*). The V_π of such a modulator can be expressed as

$$V_\pi = \frac{\lambda h}{n^3 r_{33} L \Gamma} \quad (1)$$

where λ is the optical wavelength, h is the gap between electrodes, n is the index of refraction, r_{33} is the EO coefficient of the polymer waveguide layer, L is the interaction length, and Γ is a modal overlap integral. Low V_π can be achieved by adjusting one or several parameters in Eq. 1. However, many factors such as reducing gap distance or increasing interaction length are limited by optical insertion loss and modulation frequency requirements. The most effective approach for low V_π is to increase the EO coefficient r_{33}, which is directly proportional (in the limit of no intermolecular electrostatic interactions) to the product of molecular dipole moment (μ) and the hyperpolarizability β with the number density N of the nonlinear chromophores in the polymer matrix. In this first-order approximation, the higher the $\mu\beta$ and N, the higher the EO coefficient. However, for chromophores with large dipole moments and polarizabilities (α), intermolecular electrostatic interactions among the chromophores become a

[1]TACAN Corporation, 2330 Faraday Avenue, Carlsbad, CA 92008, USA. [2]Loker Hydrocarbon Research Institute and Department of Chemistry, University of Southern California, Los Angeles, CA 90089, USA. [3]Center for Photonic Technologies, Department of Electrical Engineering, University of Southern California, Los Angeles, CA 90089, USA. [4]Department of Chemistry, University of Washington, Seattle, WA 98195, USA.

major barrier to achieving high EO coefficients at high chromophore loadings (*1*, *7*).

For dipole moments greater than 10 Debye and α values greater than 10^{-22} cm^3, intermolecular interactions can extend over considerable distances (>1 nm). At modest concentrations of chromophores [typically 20 weight % (wt %) in the polymer matrix], electrostatic interaction energies can exceed thermal energies. Even for spherically symmetric chromophores, the effect of intermolecular electrostatic interactions among chromophores is to favor overall centrosymmetric ordering of chromophores. Theoretical calculations (*1*, *7*) predict that r_{33} will exhibit a maximum, as a function of N, that will shift to lower N with increasing μ and α (Fig. 2). Theoretical calculations explicitly considering the effects of chromophore shape (*1*, *7*) predict that the attenuation of desired noncentrosymmetric order will be most severe for chromophores of prolate ellipsoidal shape (Fig. 2). Indeed, as the major-to-minor axis ratio is increased (for constant chromophore volume), the position of the maximum shifts to lower number density (Fig. 2). Thus, a simple design strategy is suggested by theoretical analysis. Derivatization of chromophores with bulky groups that inhibit close approach along the minor axes of the chromophore should result in an increase in the maximum realizable EO activity. We have sought to test this theory by derivatizing chromophores with bulky substituents (*1*, *6*). In all cases, including the examples presented here (Figs. 1 and 2), we have observed significant enhancements in the maximum achievable EO activity (*7*).

We have also incorporated an optical push-pull modulator architecture (*12*) in the design of our low V_π device. A new electrode implementation can achieve optical push-pull while minimizing the processing steps and preventing air dielectric breakdown. This electrode design also exploits the processing flexibility afforded by polymers in that the molecular alignment orientation can be defined arbitrarily by the applied electric field. During electric field poling, the chromophores in the two interferometer arms are aligned in opposite directions by the poling field (Fig. 3A). The modulation drive signal is applied to the top electrode, while the two bottom electrodes are grounded. The driving field is along the poling direction in one arm and against the poling direction in the other arm (Fig. 3B). The index modulations in the two arms are always of opposite sign and, therefore the total phase difference is twice as large as that in the single arm modulation case. The V_π is reduced by a factor of 2 as compared to that in Eq. 1. Because no other device parameters are changed in an optical push-pull modulator design, the reduced V_π is achieved without compromising performance. The three-section poling and driving electrodes can be easily adapted to a high-speed microstripline with a split ground electrode for wideband application (*13*).

To demonstrate application of the CLD-1 chromophore and optical push-pull in optical intensity modulators, we have fabricated several modulator chips using a CLD-1/poly-(methylmethacrylate) (PMMA) guest-host system (30 wt %) as an active waveguide material. The modulator chips consist of a 3.2-μm-high polyurethane lower cladding layer, a 1.4-μm-high CLD-1/PMMA guiding layer, and a 2.9-μm-high ultraviolet light–curable upper cladding layer. The waveguides and electrode arrangements were fabricated like the cross-section view in Fig. 3. After cooling down to room temperature and re-

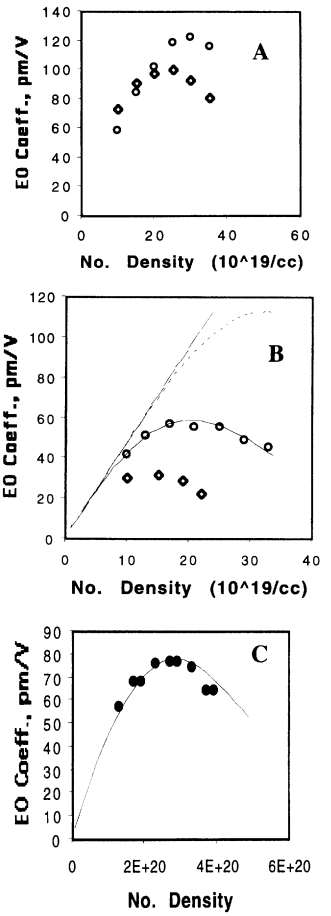

Fig. 2. Graphs of r_{33} as a function of chromophore number density are shown for several CLD- and FTC-type chromophores (Fig. 1). (**A**) Data for CLD-2 (circles) and CLD-3 (diamonds) show the effect of chromophore shape on maximum achievable r_{33}. The μβ values are somewhat different for CLD-2 and CLD-3, making the initial slopes of the curves different. (**B**) Analogous data for FTC-1 (diamonds) and FTC-2 (circles) chromophores, again showing the influence of chromophore shape on achievable EO activity. Also shown are theoretical simulations assuming no intermolecular electrostatic interactions (solid straight line), full intermolecular interactions with chromophores treated as spheres (dashed line), and full intermolecular interactions with chromophores treated as ellipsoids (solid curving line). The ellipsoidal shape was defined by Spartan (WAVEFUNCTION, Inc., Irvine, California) calculations. (**C**) Experimental (solid circles) and theoretical (solid line) data compared for a variant of CLD-1, where the OTBDMS (tetrabutyldimethylsiloxane) protecting group has been replaced by a methoxy group. The theoretical curve was computed without adjustable parameters and explicitly incorporates nuclear repulsive interactions (as well as electronic interactions) treating chromophores as ellipsoids. The somewhat poorer agreement [relative to the FTC simulation of (B)] reflects neglect of higher order self-consistency (medium dielectric) effects in the calculations. Experimental data were taken at 1060 nm.

Fig. 1. Structures and abbreviated names of the chromophores discussed here. OTBDMS stands for the tetrabutyldimethylsiloxane protecting group; OAc stands for the acetate protecting group.

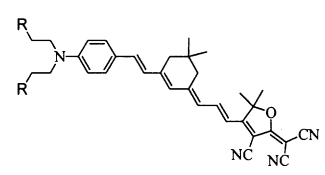

CLD-1 R = OTBDMS

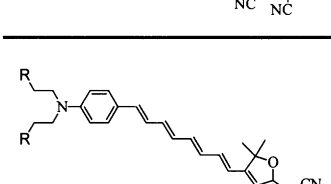

CLD-2 R = H

CLD-3 R=H

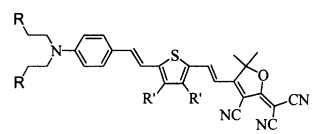

FTC-1 R = OAc, R' = H

FTC-2 R = OAc
R' = $CH_2CH_2CH_2CH_3$

moving the applied poling field, modulator V_π at low frequency (330 Hz) was measured on a waveguide test bench with a 1318-nm diode-pumped Nd–yttrium-aluminum-garnet laser source. The modulator chip characteristics are summarized in Table 1. From Table 1, the average $V_\pi L$ products were 2.46 V·cm and 2.16 V·cm for modulators with 3-cm and 2-cm interaction lengths, respectively. The difference in $V_\pi L$ can be attributed to different applied poling voltages. An EO coefficient over 60 pm/V was achieved at 1318 nm, in agreement with measured r_{33} values based on two-level model (*14*) extrapolation to 1318 nm. A digital oscilloscope trace showing a V_π = 0.769 V is shown in Fig. 4.

Modulator performance parameters other than V_π also affect the link gain and noise figure, and a complete engineering evaluation requires measurement of a broad range of parameters. The objective of this report is to point out the significant improvements in EO coefficients in a device-quality material and the achievement of very low V_π in a structure that is compatible with high-speed operation. However, we have also characterized the optical loss of the structurally modified CLD-1 chromophore/PMMA material. Typical waveguide losses were 1 decibel (dB)/cm at 1300 nm and 1.6 dB/cm at 1550 nm, measured by a sliding liquid prism method (*15*, *16*). Based on the measured loss in this material (and in other polymers containing the CLD chromophore) and assuming a 3-cm-long device with ~1-dB coupling loss at the fiber input and output (*1*), an insertion loss of ~6 dB is predicted for the polymer devices (*17*). This value is close to that of commercial lithium niobate modulators. Because of the low glass transition temperature (T_g) of PMMA, the thermal stability of the modulator reported here is only about 65°C. However, we have recently prepared modulators using a higher T_g polymer {poly[bisphenol A carbonate-co-4,4′-(3,3,5-trimethylcyclohexylidene) diphenol], amorphous poly(carbonate) (APC), T_g = 205°C}, which increases the thermal stability of EO activity to >100°C. Because of the higher dielectric constant of APC, somewhat higher EO coefficients are obtained, as predicted by theory. We have also prepared double-end–cross-linkable (DEC) variants of CLD-1 that exhibit thermal stability in excess of 120°C. These DEC materials also exhibit good stability in the presence of 1300-nm light and gamma radiation. However, heavily cross-linked CLD-containing DEC materials have yet to be evaluated in devices. Even in the relatively soft materials reported here, we have observed no photodecomposition for the modest power levels used; the same observation holds for the Lockheed-Martin studies (*9*).

Like other EO modulators, V_π is expected to increase as the modulation frequency increases. The increase in V_π at high frequencies is due to two factors: the velocity mismatch between the optical wave and the rf wave, and the rf loss of the traveling wave structure. The inherent advantage of the polymers is the relatively low difference in wave velocity between the optical and rf waves. Mismatch effects are therefore not seen in typical polymer devices until modulation frequencies of over 100 GHz are used. Specially designed traveling wave structures can be used to overcome the velocity mismatch in crystalline modulators, but this typically reduces the overlap between the rf and optical fields and results in an increased V_π. On the other hand, the polymer devices, even up to 100 GHz, remain simple microstrip line structures with a high overlap integral. The rf loss is typically determined by the conductivity of the metal electrodes and is independent of the EO material used (*18*). The V_π typically increases by a factor of 2 at ~40 GHz as compared to the low frequency value for a device with an interaction length of 2 to 3 cm. Bias point stability can be achieved with the use of electrically compatible polymer cladding layers in the modulator (*19*). No bias point instability has been observed for the modulators discussed here, but this point needs to be addressed in a carefully controlled test over a substantial period of time under actual practical operating conditions.

The V_π reported here proves the long awaited feasibility of sub–1-V V_π devices. Polymer modulators can be directly integrated with the fastest very-large-scale integration (VLSI) electronics without the use of low-noise (and bandwidth-limiting) amplifiers. Thus, the stage is set for exploitation of the recently demonstrated integration of VLSI electronics and polymer modulators to fabricate high-bandwidth optochips (*1*, *20*). Moreover, our current results must be viewed in the context that we have recently prepared chromophores that when incorporated into PMMA and APC polymer matrices yield r_{33} values approximately twice those of CLD-1 (nearly four times that of lithium niobate) at telecommunication wavelengths (*21*). Optical loss is comparable to that obtained for CLD-1–containing materials, and thermal stability is actually improved (*21*). These new materials involve incorporation of dithiophene units in the chromophore bridge or extending the isophorone structure by use of multiple fused rings (*21*). Steric modification has been used to both inhibit unwanted intermolecular electrostatic interactions and to increase the planarity (π-orbital overlap) of the π-electron system. However, these materials have yet to be incorporated into devices and evaluated under device-relevant conditions; numerous processing issues must be addressed. Although final judgment must be withheld concerning the detailed performance limits of polymer modulators, there is good reason to anticipate considerable improvement in the near future. Practical implementation of sub–1-V EO polymer modulators will open up wide applications for polymeric materials, including direct

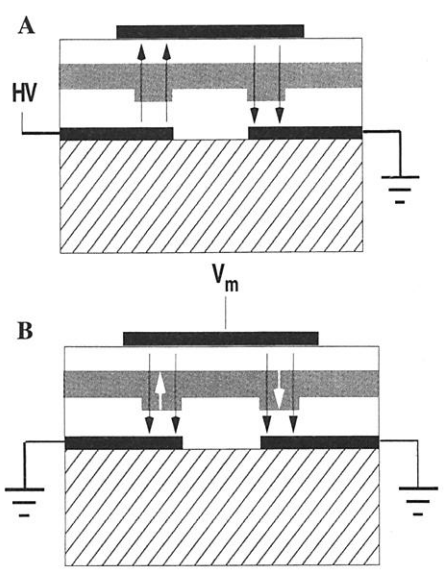

Fig. 3. Schematic cross sections of polymer modulator electrodes and waveguide layers. **(A)** Push-pull poling. **(B)** Push-pull driving. V_m is the modulation or driving voltage. The black arrows indicate local electric field direction. The white arrows indicate local chromophore orientation.

Table 1. Operational characteristics of polymeric modulators.

Parameters	MZ094 chip	MZ096 chip
Interaction length (cm)	3.0	2.0
Total film thickness (μm)	7.3	7.3
Poling voltage (V)	500	750
Poling temperature (°C)	87	87
Devices per chip	6	6
Optical wavelength (nm)	1318	1318
Measured V_π range (V)	0.77–0.93	1.03–1.10
Average V_π (V)	0.82	1.08
Average r_{33} (pm/V)	57.8	65.6
Measurement uncertainty	<10%	<10%

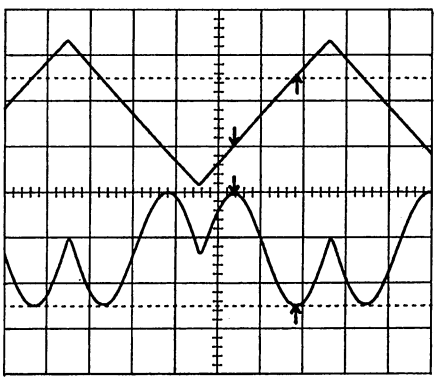

Fig. 4. A V_π measurement snapshot showing a V_π = 0.77 V. The measured V_π is displayed as the voltage difference (a channel 2 reading of 769 mV) between two cursors on the upper trace. The positions of the two cursors are determined by the two turning points on the modulator output waveform (lower trace). The *x*-axis time divisions correspond to 500 μs. Data are for a wavelength of 1318 nm.

integration with high-speed electronic circuits (*1*, *20*) and the realization of lossless microwave links.

References and Notes

1. L. R. Dalton *et al.*, *J. Mater. Chem.* **9**, 1905 (1999); B. H. Robinson *et al.*, *Chem. Phys.* **245**, 35 (1999); W. H. Steier *et al.*, *Chem. Phys.* **245**, 487 (1999); H. S. Nalwa and S. Miyata, Eds., *Nonlinear Optics of Organic Materials and Polymers* (CRC Press, Boca Raton, FL, 1998); J. Zyss, Ed., *Molecular Nonlinear Optics* (Academic Press, New York, 1994); D. L. Wise *et al.*, Eds., *Electrical and Optical Polymer Systems* (Dekker, New York, 1998); P. N. Prasad and D. Williams, *Introduction to Nonlinear Optical Effects in Molecules and Polymers* (Wiley, New York, 1991).
2. W. E. Stephens and T. R. Joseph, *J. Lightwave Technol.* **5**, 380 (1987); C. H. Cox, G. E. Betts, L. M. Johnson, *IEEE Trans. Microwave Theory Tech.* **38**, 501 (1990).
3. C. C. Teng, *Appl Phys. Lett.* **60**, 1538 (1992); D. Chen *et al.*, *Appl Phys. Lett.* **70**, 3335 (1997); H. Fetterman *et al.*, in *Organic Optics and Optoelectronics* (1998 IEEE/LEOS Summer Topical Meeting Digest, Institute of Electrical and Electronic Engineers, New York), pp. 9–10; W. Wang *et al.*, *Appl. Phys. Lett.* **67**, 1806 (1995).
4. K. Naguchi, O. Mitomi, H. Miyazawa, *J. Lightwave Technol.* **16**, 615 (1998).
5. W. K. Burns *et al.*, *IEEE Photon. Technol. Lett.* **10**, 805 (1998).
6. S. R. Marder, D. N. Beratan, L. T. Cheng, *Science* **252**, 103 (1991); S. R. Marder and J. W. Perry, *Science* **263**, 1706 (1994); S. R. Marder *et al.*, *Science* **265**, 632 (1994); D. R. Kanis, M. A. Ratner, T. J. Marks, *Chem. Rev.* **94**, 195 (1994); I. D. L. Albert, T. J. Marks, M. A. Ratner, *J. Am. Chem. Soc.* **119**, 6575 (1997).
7. L. R. Dalton, A. W. Harper, B. H. Robinson, *Proc. Natl. Acad. Sci. U.S.A.* **94**, 4842 (1997).
8. C. Zhang *et al.*, *Polym. Prepr.* **40**, 49 (1999).
9. S. Ermer *et al.*, *Proc. SPIE*, in press.
10. H. Lee *et al.*, *Appl. Phys. Lett.* **71**, 3779 (1997).
11. Y. Shi *et al.*, *IEEE J. Sel. Top. Quantum Electron.* **2**, 289 (1996); Y. Shi, W. Wang, D. J. Olson, W. Lin, J. H. Bechtel, *Proc. SPIE* **3632**, 144 (1999).
12. W. Wang *et al.*, *IEEE Photon. Technol. Lett.* **11**, 51 (1999); T. A. Tumolillo and P. R. Ashley, *IEEE Photon. Technol. Lett.* **4**, 142 (1992); K. H. Hahn *et al.*, *Electron. Lett.* **30**, 1220 (1994).
13. H. R. Janson, *Arch. Elektronik Übertragungstechn.* **32**, 485 (1978).
14. K. D. Singer, M. G. Kuzyk, J. E. Sohn, *J. Opt. Soc. Am. B* **4**, 968 (1987).
15. C. C. Teng, *Appl. Opt.* **32**, 1051 (1993).
16. We have recently realized even lower loss values in partially halogenated materials (for example, 0.7 dB/cm at 1300 nm and 1.0 dB/cm at 1550 nm).
17. Coupling losses of less than 1 dB have been realized by means of exploiting mode size matching techniques and vertical transition waveguide structures [S. M. Garner *et al.*, *IEEE J. Quantum Electron.* **35**, 1146 (1999)]. The total insertion loss of a commercial (Pacific Wave Industries, Los Angeles, CA) EO modulator based on the CLD-1 chromophore is comparable to that of the Lucent lithium niobate modulator.
18. D. Chen *et al.*, *IEEE Photon. Technol. Lett.* **11**, 54 (1999).
19. H. Park, W. Hwang, J. Kim, *Appl. Phys. Lett.* **70**, 2796 (1997); Y. Shi, W. Wang, W. Lin, D. J. Olson, J. H. Bechtel, *Appl. Phys. Lett.* **71**, 2236 (1997).
20. S. Kalluri *et al.*, *IEEE Photon. Technol. Lett.* **8**, 644 (1996).
21. As can be seen from Fig. 2, even modest modification of the structure of CLD-1 can lead to significant improvement in optical nonlinearity. A particularly attractive route to increasing conjugation length while maintaining exceptional thermal and photochemical stability is the insertion of dithiophene units I. Liakatas *et al.*, *Appl. Phys. Lett.*, **76**, 1368 (2000); L. R. Dalton *et al.*, U.S. Patent pending.

22. Research supported by Air Force Research Laboratory, Air Force Office for Scientific Research, Ballistic Missile Defense Organizations, National Science Foundation, and Office of Naval Research.

15 September 1999; accepted 25 February 2000

REPORTS

Dilational Processes Accompanying Earthquakes in the Long Valley Caldera

Douglas S. Dreger,[1]* Hrvoje Tkalčić,[1] Malcolm Johnston[2]

Regional distance seismic moment tensor determinations and broadband waveforms of moment magnitude 4.6 to 4.9 earthquakes from a November 1997 Long Valley Caldera swarm, during an inflation episode, display evidence of anomalous seismic radiation characterized by non–double couple (NDC) moment tensors with significant volumetric components. Observed coseismic dilation suggests that hydrothermal or magmatic processes are directly triggering some of the seismicity in the region. Similarity in the NDC solutions implies a common source process, and the anomalous events may have been triggered by net fault-normal stress reduction due to high-pressure fluid injection or pressurization of fluid-saturated faults due to magmatic heating.

The Long Valley Caldera (LVC) of eastern California (Fig. 1) is tectonically and volcanically active. The 15-km-wide and 30-km-long caldera has produced numerous eruptions since the penultimate event 730,000 years ago that ejected 600 km^3 of rock and formed the caldera through subsequent collapse. The current seismic unrest in the LVC began in 1980 with episodic earthquake swarms and the inflation of a resurgent dome (*1*) (Fig. 1). As a result of this activity the U.S. Geological Survey initiated extensive seismic, ground deformation, and chemical monitoring in 1982. These surveys have revealed episodic seismicity swarms that correlate with the inflation of the resurgent dome, but confirmation of direct fluid involvement in the seismicity has been elusive.

In May 1980, four magnitude (M) 6 earthquakes occurred: two south of the LVC in the vicinity of the Hilton Creek fault, and two in the south moat of the caldera (Fig. 1). Two of these events, one located at the caldera margin and the other 12 km to the south, as well as an earlier event in 1978, were found to have significant non–double couple (NDC) seismic moment tensors (*2*).

The latest episode of LVC deformation began in 1997 and first became apparent in two-color laser geodimeter data as increased inflation of the resurgent dome in June followed by earthquake swarm activity in the south moat in July. Deformation rates and swarm activity continued to increase through October to rates exceeding 2 cm/month and 100 $M > 1.2$ earthquakes per day. Swarm activity, strain, and tilt rates increased on 22 November 1997, with the onset of a series of $M > 4$ earthquakes. A borehole strain meter recorded a transient signal over the next week. Dome inflation, deformation, and swarm activity returned to background rates in early 1998 (*3*).

We investigated anomalous radiation characteristics of the 1997 earthquake swarm using a moment tensor methodology. The seismic moment tensor, Mij, provides a general representation of the seismic source and can be determined by the linear inversion of observed seismic ground motions with appropriately calibrated Green's functions (*4*). Mij is commonly decomposed into double couple (DC), compensated-linear-vector-dipole (CLVD), and isotropic components (*5*), where each of the components of the moment tensor decomposition is represented as a percentage of the total (*6*). The DC consists of two vector dipoles of equal magnitude but opposite sign, resolving shear motion on faults oriented 45° to the principle eigenvectors of Mij. The CLVD consists of a major vector dipole with twice the strength and opposite sign to two orthogonal, minor vector dipoles and can describe the separation or compression of a fault with no net volume change. The isotropic component has three orthogonal vector dipoles of equal magnitude and resolves volumetric changes.

NDC seismic moment tensors have been observed in a variety of tectonic and volcanic environments. Several mechanisms such as multiplanar rupture (*7*, *8*), nonplanar rupture (*9*), and tensile failure (*10*) have been proposed to explain observed NDC moment tensors. In principle it should be possible to determine the isotropic components given body and surface wave data; however, they are difficult to resolve (*11*), and only a few studies have reported significant volumetric components (*12*, *13*).

Routine analysis of seismic moment tensors by the Berkeley Seismological Laboratory revealed that a number of events in the November 1997 swarm displayed unusual seismic radiation patterns (*14*). Seven events (Table 1) have

[1]Berkeley Seismological Laboratory, University of California, Berkeley, CA 94720, USA. [2]U.S. Geological Survey, Menlo Park, CA 94025, USA.

*To whom correspondence should be addressed at Berkeley Seismological Laboratory, 281 McCone Hall, University of California, Berkeley, CA 94720, USA. E-mail: dreger@seismo.berkeley.edu